Available online at www.sciencedirect.com

ScienceDirect

Energy Procedia 38 (2013) 760 – 769

Energy Procedia

SiliconPV: March 25-27, 2013, Hamelin, Germany

Recombination and microstructural properties of soldering pads and their impact on solar cell performance

Karin Krauß*, Fabian Fertig, Stefan Rein

Fraunhofer Institut for Solar Energy Sytems (ISE), Heidenhofstraße 2, 79110 Freiburg, Germany

Abstract

The recombination induced by soldering pads, screen printed with a commercially available paste containing primarily silver and an aluminium amount of 1-5 $\%_{wt}$, is investigated concerning the open-circuit voltage for aluminium back surface field (Al-BSF) solar cells. The saturation current density $J_{o,pad}$ due to soldering pads is found to be in the range of $26.7 \cdot 10^3$ to $85.4 \cdot 10^3$ fA/cm^2 for different conditions of the rear silicon surface. The recombination under soldering pads leads to a voltage drop of ΔV_{oc} = 6.7 mV for Al-BSF solar cells with 6.2 % of the rear side being covered with soldering pads compared to a cell with full-area Al-BSF. Within a microstructural analysis of the interface between the silicon surface and the soldering pads it is found that Al-alloying from the Al share in the soldering pad paste only occurs insularly. Furthermore, Al-BSF cells with and without residual rear side emitter and varying area fraction of soldering pads, using a soldering pad paste with and without an Al-share, are investigated. It is found that the non-overcompensated emitter regions under the soldering pads of Al-BSF solar cells affect cell performance dramatically in case of full area soldering pad, especially for an Al-free pad paste.

Keywords: Solar cells; Metallization; Recombination; Loss analysis

1. Introduction

Since pure aluminium (Al) is not solderable by standard soldering techniques, soldering pads are integrated into the layout of the solar cells' rear side. Soldering pads are screen printed with special pastes containing a high amount of silver or exclusively silver to provide good soldering properties. While the formation of the highly Al-doped p^+-region – formed at the rear by alloying of silicon and Al-pastes in a co-firing step and known as back-surface field (BSF) – has been the topic of extensive research [1-3],

* Corresponding author. Tel.: +49-(0)761-4588-5656; fax: 49-(0)761-4588-9250.
E-mail address: karin.krauss@ise.fraunhofer.de.

doi:10.1016/j.egypro.2013.07.344

soldering pads are only rarely addressed in experimental studies on microstructural and electrical properties. However, a reduction of the soldering pads' area fraction is reported to be beneficial for the open-circuit voltage in addition to the cost advantage due to the lower silver consumption [4].

In this work, we investigate the recombination induced by soldering pads which are screen printed with a commercially available paste containing an Al amount of 1-5 $\%_{wt}$. and determine the resulting losses in open-circuit voltage for Al-BSF cells. Furthermore, the interface between soldering pads and silicon is subjected to a microstructural analysis. Since the microstructural analysis in section 3 points towards a partially insular Al-alloying, section 4 addresses the question how a residual rear-side emitter which is not or only partially over-compensated by Al-alloying under the soldering pads affects solar cell performance. Therefore, Al-BSF solar cells with and without residual rear-side emitter and varying area fraction of the soldering pads on the cells' rear side are produced. In order to investigate the effect of partial Al-alloying from the Al share in the soldering pad paste, an Al-free soldering pad paste was used in addition to the soldering pad paste investigated in the experiment on recombination and microstructural properties with an Al share of 1-5 $\%_{wt}$.

2. Recombination under soldering pads

2.1. Sample preparation

The test samples for the recombination study have been processed on 10 Ωcm *p*-type float zone silicon (FZ-Si) wafers with high bulk lifetimes to ensure that the total recombination of the test structure is only limited by surface recombination. The chosen test structure is asymmetric. The front side is masked with a thermal oxide, which acts as texture and diffusion barrier. Hence, the front surface remains shiny etched and non-diffused, which enables optimum front surface passivation. On the rear side two different surface conditions are prepared, which are motivated in the following. The rear side of Al-BSF cells is usually textured and diffused with a parasitic phosphorous emitter, in case of a processing sequence without chemical edge isolation. For our test samples, this specific surface condition is prepared by an alkaline texture and subsequent tube furnace diffusion with $POCl_3$. In order to investigate the influence of the phosphorous emitter and the texture-induced surface enlargement on the properties of the interface between silicon and soldering pad, a smooth surface without emitter diffusion is prepared by a simple saw damage etch. This surface condition will be referred to as surface condition A (SC A) distinguishes itself from the textured surface with emitter, which will be referred to as surface condition B (SC B).

After preparation of the rear surface conditions of the test samples, the oxide mask at the front side is removed and the front side is coated with a passivating SiN layer. Following this, both types of wafers (SC A and B) are divided into two groups each, so that each group is represented by four test samples. Group 1 is screen printed with a full area soldering pad using a commercially available soldering pad paste containing primarily silver and an aluminium amount of 1-5 % wt. In contrast to that, group 2 is screen printed full area with a commercially available Al-BSF paste in order to determine the saturation current density $J_{o,bsf}$ of the highly Al-doped p^+-region, which accounts for the larger area fraction of the solar cells rear side and thus reflects a desirable lower benchmark for the saturation current density under the soldering pads.

Simulating the co-firing step used for the contact formation of Al-BSF cells, the samples are fired in an industrial conveyor belt furnace. We adjusted the pre-set peak temperatures which individually for wafers with different metallization, so that the same wafer temperatures are reached. In a last step, metal paste residuals and eutectic layers are removed in a solution of hydrochloride acid (HCl) or a solution of HCl and subsequent etching in a solution of nitric acid (HNO_3) for wafers with Al paste or soldering pad paste, respectively.

In order to determine the saturation current densities $J_{o,bsf}$ of the highly Al-doped p^+-region and $J_{o,pad}$ induced under soldering pads, quasi-steady state photoconductance (QSSPC) measurements are performed. For the analysis of the microstructural properties of the interface scanning electron microscopy (SEM) measurements are carried out.

2.2. Determination of the saturation current density from QSSPC measurements

The saturation current densities of the highly Al-doped p^+-regions are extracted from QSSPC measurements according to a procedure described in Refs. [5-8]. However, the method had to be adapted for the test samples screen printed with soldering pads since high-level injection could not be reached in the QSSPC measurements [6] for those samples. Instead we are using the expression

$$\frac{1}{\tau_{\mathrm{eff}}} = \frac{1}{\tau_{\mathrm{bulk}}} + \left[\frac{W}{S_{\mathrm{rear}}} + \frac{4}{D_{\mathrm{n}}} \left(\frac{W}{\pi} \right)^2 \right]^{-1} \tag{1}$$

given by Sproul et al. [9] for the measured carrier lifetime τ_{eff} of the samples. Eq. (1) is valid if the surface recombination velocity of one side, in this case S_{rear}, is dominating the surface recombination, that is $S_{\mathrm{rear}} >> S_{\mathrm{front}}$. Auger recombination in the bulk is accounted for in τ_{bulk} by using the parametrization given by Kerr et al. [10], W denotes the sample thickness and D_{n} the minority carrier diffusion constant. Solving Eq. (1) for S_{rear} and using this expression in the general expression [11] for the saturation current density under low-level injection ($\Delta n << N_{\mathrm{A}}$) for the base doping density N_{A} of the test samples, the saturation current density $J_{\mathrm{o,rear}}$ of the rear side of an asymmetrical sample (given $S_{\mathrm{rear}} >> S_{\mathrm{front}}$) can be written as

$$J_{\mathrm{o,rear}} = S_{\mathrm{rear}} \frac{q n_i^2}{N_A} = \frac{q n_i^2 W}{N_A} \left[\left(\frac{1}{\tau_{\mathrm{eff}}} - \frac{1}{\tau_{\mathrm{bulk}}} \right)^{-1} - \frac{4}{D_{\mathrm{n}}} \left(\frac{W}{\pi} \right)^2 \right]^{-1} \tag{2}$$

with the elementary charge q and the intrinsic carrier concentration n_{i}.

Since the front side of the test samples is passivated with SiN yielding a surface recombination velocity of $S_{\mathrm{front}} \approx 14$ cm/s, which has been measured on symmetrical passivation test samples which were processed in parallel as reference, the prerequisite $S_{\mathrm{pad}} >> S_{\mathrm{SiN}}$ for Eq. (1) and (2) is fulfilled and $J_{\mathrm{o,pad}}$ can be calculated with Eq. (2) from the measured lifetime under low-level injection.

2.3. Saturation current density under soldering pads

With the introduced procedures the saturation current densities $J_{\mathrm{o,rear}}$ for samples of surface conditions A (smooth without emitter) and B (textured with residual phosphorous emitter) were extracted from the QSSPC measurements and are shown in Fig. 1a for the full area Al-BSF and full area soldering pads. The saturation current density of the p^+-region is almost unaffected by the investigated variations in the

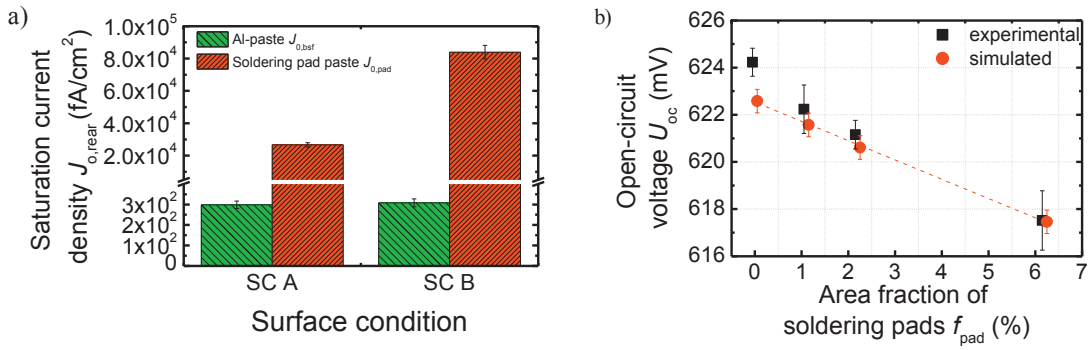

Fig. 1. a) Saturation current density $J_{o.bsf}$ and $J_{o.pad}$ for the highly Al-doped p$^+$-region and the soldering pads, respectively, measured under low-level injection. SC A denotes a saw-damage-etched rear surface without emitter and SC B a textured rear surface with emitter. Shown are the mean values and the according standard deviations of four test samples. b) Open-circuit voltages of Cz-Si Al-BSF cells with varying area fraction of soldering pads. The values simulated by means of an analytical description of the open-circuit voltage using the determined values for $J_{o.bsf}$ and $J_{o.pad}$ (circles) correspond well to the measured values (squares).

surface conditions, since the difference between $J_{o,bsf}$ = 298 fA/cm^2 for SC A and $J_{o,bsf}$ = 308 fA/cm^2 for SC B lies within the standard deviation $\delta J_{o,bsf}$ = 19 fA/cm^2 for the determined mean values. This indicates that the parasitic emitter has been completely over-compensated, and the difference in surface roughness, which may remain after alloying, does not affect the surface recombination velocity of the Al-p$^+$-region. The effect of over-compensation of a phosphorous emitter is well-known and used in solar cell fabrication [12,13]. It has also been reported [8] that a phosphorous emitter has only minor effects on the saturation current density of the Al-doped p$^+$-region, nevertheless Rauer et al. [8] reported a slightly reduced depth of the p$^+$-region when being formed on top of a phosphorous emitter.

The recombination induced by soldering pads $J_{o,pad}$ exceeds $J_{o,bsf}$ by a factor 90 to 280, reaching $J_{o,pad} = 26.7 \cdot 10^3$ fA/cm^2 for SC A and $J_{o,pad} = 85.4 \cdot 10^3$ fA/cm^2 for SC B. The increase in $J_{o,pad}$ from SC A (smooth emitter-free surface) to SC B (textured surface with parasitic emitter) may be caused by the texture induced surface enlargement and effects due to the parasitic rear side emitter, which will also be discussed in the microstructural analysis.

2.4. Impact of the soldering pads on solar cell performance

Fig. 1b displays the open-circuit voltage of Al-BSF Cz-Si solar cells with varying area fraction of the soldering pads. For the solar cells with the highest area fraction of soldering pads of f_{pad} = 6.2 %, a drop in V_{oc} of ΔV_{oc} = -6.7 mV is observed compared to solar cells with full area Al-BSF (f_{pad} = 0 %).

To showcase that the determined saturation current density $J_{o,pad}$ matches the actual recombination induced by the soldering pads, the Al-BSF Cz-Si solar cells with varying area fraction of soldering pads are modeled analytically. The minority carrier diffusion length L_n is calculated from the bulk lifetime considering the intrinsic Auger-recombination via [10] and SRH-recombination caused by the well-known Cz-specific boron oxygen complex using the parameterization from Ref. [14]. Both effects depend on bulk resistivity. The effective diffusion length L_{eff} is influenced by the diffusion length L_n and the rear surface recombination velocity S_{rear}. With the saturation current densities $J_{o,bsf}$ and $J_{o,pad}$ determined in the previous subsection, the surface recombination velocity can be calculated from the area weighted mean $J_{o,rear}$ of the saturation current densities $J_{o,bsf}$ and $J_{o,pad}$. Note that S_{rear} is proportional to N_A. The effective diffusion length is then given by [15]

$$L_{\mathrm{eff}} = L_{\mathrm{n}} \frac{1 + \frac{L_{\mathrm{n}} S_{\mathrm{rear}}}{D_{\mathrm{n}}} \tanh\left(\frac{W}{L_{\mathrm{n}}}\right)}{\frac{L_{\mathrm{n}} S_{\mathrm{rear}}}{D_{\mathrm{n}}} + \tanh\left(\frac{W}{L_{\mathrm{n}}}\right)} \quad . \tag{3}$$

The base dark saturation current density $J_{0\mathrm{b}}$ is determined via

$$J_{0\mathrm{b}} = \frac{q n_i^2 D_{\mathrm{n}}}{N_{\mathrm{A}} L_{\mathrm{eff}}} \tag{4}$$

as described in [15]. Since an increase in surface recombination velocity S_{rear} leads to lower effective bulk diffusion lengths L_{eff}, the base dark saturation current density $J_{0\mathrm{b}}$ increases. A constant emitter saturation current density of $J_{0\mathrm{e}} = 360$ fA/cm^2 is assumed for the front side emitter including higher recombining areas under the front side metallization [16] with a typical metallization fraction of 7.5 %. Using the measured short circuit current density J_{sc} of the solar cells, the one-diode model leads to the following

$$V_{\mathrm{oc,lim}} = \frac{kT}{q} \ln\left(\frac{J_{\mathrm{sc}}}{J_{0\mathrm{b}} + J_{0\mathrm{e}}} + 1\right) \tag{5}$$

expression for the theoretical value of the open-circuit voltage of the Al-BSF solar cells, with the Boltzmann constant k, the elementary charge q and the temperature T.

The results for $V_{\mathrm{oc,lim}}$ determined by Eq. (5) using the measured values for $J_{\mathrm{o,bsf}}$ and $J_{\mathrm{o,pad}}$ are displayed in Fig. 1b (red circles). As can be seen, the simulated $V_{\mathrm{oc,lim}}$ values match the actual open-circuit voltages of the solar cells quite well. As the simulated values show a linear drop of the open-circuit voltage with the area fraction of the soldering pads in the investigated range of area fractions, it may be quantified from Fig. 1b as $\Delta V_{\mathrm{oc}} \approx$ -0.8 mV per percent increase of the soldering pads' area fraction. The drop in the open-circuit voltage of the solar cells is even slightly higher, indicating that the recombination induced by the soldering pads may be even slightly higher than suspected from the determined value $J_{\mathrm{o,pad}}$. This difference may originate in effects of the assembly of the higher and less recombining areas, which the area weighted mean of $J_{\mathrm{o,pad}}$ and $J_{\mathrm{o,bsf}}$ does not account for. Nevertheless, the saturation current density is sufficient to describe the experimental data for varying area fraction of soldering pads.

3. Microstructural analysis

For the microstructural analysis, the cross sections of the samples introduced in subsection 2.1 were investigated with scanning electron microscopy (SEM).

Scanning electron microscopy is a common method to investigate Al-alloying on silicon surfaces. Since the detected signal increases with increasing doping concentration, Al-doped regions appear brighter than the silicon bulk. Krause et al. [1] presented a comprehensive microstructural analysis of Al-alloyed contacts using scanning electron microscopy. Besides the formation of Si lamellas in the eutectic Al/Si layer, the growth of pyramidal structures and self-assembled lines of those pyramidal structures on Al-p$^+$ surface was reported in their studies. These structures are assumed to be formed during the immediate solidification of the liquid Al/Si phase when the eutectic point $T_{\mathrm{eut,Al\text{-}Si}} = 577$ °C in the cooling-down phase of co-firing is reached [1]. An additional profound study by Bock et al. [17] came to the conclusion that these structures appear over Al inclusions lying 50 nm underneath the silicon surface.

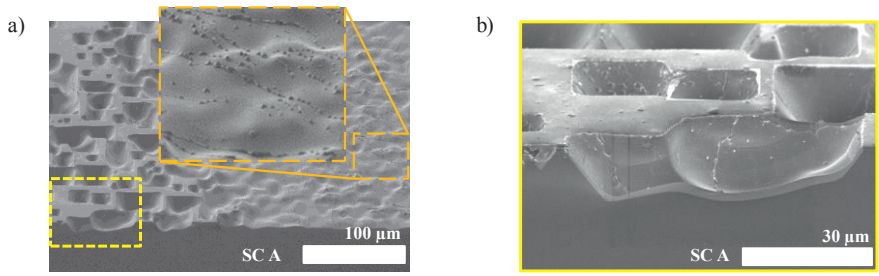

Fig. 2. SEM-images of a sample with surface condition A, screen printed with Al paste after co-firing and HCl etching. a) Tilted view on the Al-p^+ surface under an angle of 34°. Near the wafer edge (left side) where Al spalled during co-firing planar surface remain and etch pits appear in between on the surface. Towards the wafer center (right side) where the Al contact formed well a typical p^+-surface can be seen. b) In the cross-sectional view of the etch pit region on a larger scale, an Al- p^+-region with a thickness of $d_{p+} \approx 2$ µm can be seen underneath an etch pit.

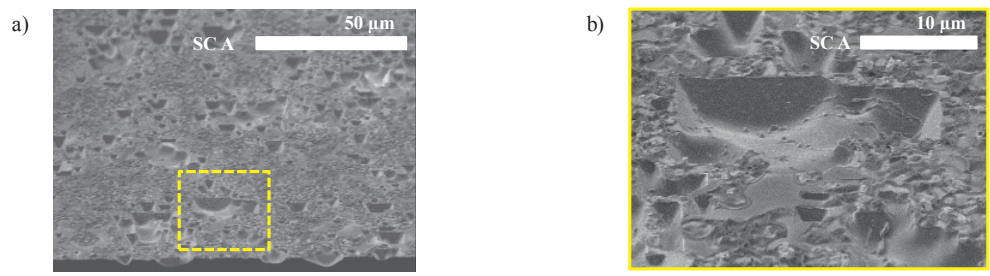

Fig. 3. SEM-images of a sample screen printed with soldering pad paste after co-firing and HCl/HNO_3 etching under an angle of 34°. a) All over the surface etch pits are observed. b) The zoom shows an etch pit with typical characteristics of an Al-p^+ surface.

3.1. Surfaces and cross-sections after metal etch-off

In Fig. 2, a sample with surface condition A which has been screen printed full area with Al-paste is shown after co-firing and HCl etching. The tilted view on the surface in Fig. 2a can be divided in a left and a right side showing two different characteristics. On the right hand side of the SEM -image, a typical structure of an Al-p^+ surface can be seen, showing self-assembled lines of pyramidal structures as reported in Refs. [1,17]. However, approaching the wafer edge on the left hand side, there is a remaining smooth surface filled with etch pits, that appeared after the HCl etch. A partial spalling of the Al-paste near the wafer edge during co-firing was observed for these samples. In places, where Al spalled, no alloy was formed and a smooth surface remained. However, the irregular appearance of etch pits indicates, that in insular small areas Si was dissolved in liquid Al during the co-firing, forming a eutectic layer in these areas. After the removal of the eutectic layer and paste residuals those etch pits attest a partial Al-alloying. Fig. 2b gives a closer cross-sectional view at one of the etch pits. Furthermore, a p^+-region with a thickness up to $d_{p+} = 2$ µm has been formed under this etch pit as can be seen in Fig 2b. The question arises if it is possible to induce Al-alloying from the Al share of 1-5 % wt. in the soldering pad paste during co-firing. In contrast to an Al-paste, there is the presence of silver in the paste, and maybe even changed amounts of chemical components, such as glass frit, in the paste, which may act as obstacles to Al-alloying.

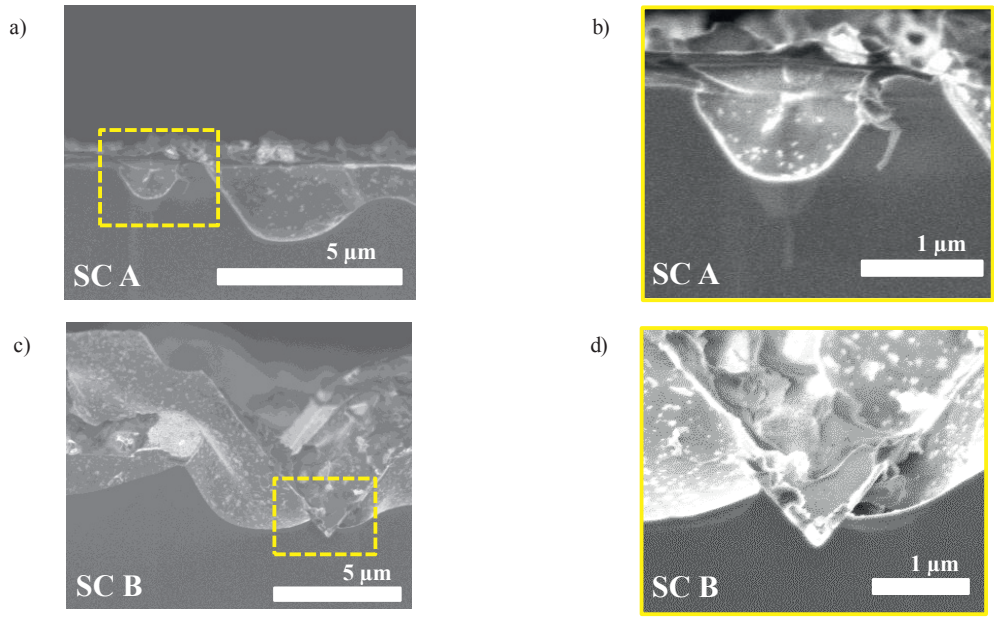

Fig. 4. SEM-images of the test samples cross sections after metal etch off. The two investigated samples were both screen printed with the soldering pad paste but distinguish themselves in the rear surface conditioning: (upper row, SC A) planar surface without emitter, (lower row, SC B) textured surface with emitter. **(a)** The surface of the SC A samples remains planar after alloying with some etch pits. **(b)** Zoom into a small etch pit of the sample from (a) with SC A surface; which shows a 0.5 µm deep area with higher signal in its extension, which points towards Al-doping by the Al share in the soldering pad paste. **(c)** The surface of the SC B samples is rougher and has larger height differences after alloying than the surface of the SC B samples. Even a structure reminding on the edges of the random pyramids remains. **(d)** Where the sharp line of the cross section changes into a smoothly shaped line, a little light shadow can be seen right under the surface, indicating a possible Al-doping.

In Fig. 3, SEM-images of a test sample with surface condition A which has been screen printed with soldering pad paste ($f_{pad} = 0\,\%$) are shown after co-firing and HCl/HNO_3 etching. As can be seen in Fig. 3a, etch pits similar to the ones in Fig 2 developed under spalled Al-paste are randomly distributed over the surface. Nevertheless, the etch pits developing under the soldering pad paste have about half the width of the ones which developed in areas of spalled Al paste. In a closer look, given in Fig. 3b, one can even see rudimentary traces of self-assembled line structures indicating possible Al-inclusions.

Finally, Fig. 4 gives a cross-sectional view on samples with SC A (a-b) and SC B (c-d) which have been screen printed with soldering pad paste the SEM-images taken after firing and HCl and HNO_3 etching. As can be seen in Fig. 4a, on the smooth SC A surface etch pits with a depth up to 2 µm are formed. In the zoom of the smaller etch pit shown in Fig. 4b, a bright area can be seen in the extension of the etch pit pointing towards a higher doping in this area. However, for the textured SC B surface shown in Fig. 4c, etch pits cannot be identified as clearly as for the SC A surface, since the SC B surface is still rather rough after Al-alloying. In fact, the SEM-image shows two edges, which seem to originate in the same point and may be remaining edges of two pyramids from the alkaline texture. However, zooming into the cross section in Fig. 4d, the surface on the right and left side of the inverted tip built by the two remaining pyramid edges describes smooth concave lines. These concave structures are most likely the residuals of etch pits which formed on the tilted pyramid planes by etching off an eutectic layer near the pyramid surface as on the planar SC A surface. Underneath these concave structures, the SEM-image

exhibits a thin layer which appears brighter and thus represents a highly doped region, which supports the assumption that an alloying took place in those spots.

Since the wafer temperature reached at maximum is below the melting point of silver $T_{melt,Ag} = 961.93$ °C and below the eutectic point of an Ag/Si system $T_{eut,Ag/Si} = 835$ °C [18], it is ensured that no liquid Ag/Si phase exists at any time during co-firing. However, there is the possibility of Ag dissolving in the liquid Al/Si phase, which is formed by melting of the Al-share in the soldering pad paste during co-firing. But due to the low solubility of Ag in liquid Al [19], the Ag content in the liquid Al/Si phase should be negligible. Thus, brighter areas under the silicon surface in Fig. 4a-d may be assigned to Al-doping from the Al-share in the soldering pad paste.

To sum up, the microstructural analysis showed that etch pits in the surface after HCl or HCl and HNO_3, etching, respectively, originate from Al-alloying and the formation of a eutectic layer during co-firing. Pyramidal structures typical for Al-p^+ surfaces were observed in the etch pits as well. This leads to the conclusion, that an Al-alloying from the 1-5 % wt. Al-share in the soldering pad paste took place.

4. Overcompensation of a residual phosphorous emitter under soldering pads

Since the microstructural analysis in the previous section showed that the Al-alloying from the Al-share in the soldering pad paste only occurs insularly, there is still a residual phosphorous emitter under the soldering pads of Al-BSF cells if a processing sequence without chemical edge isolation is used. In order to investigate the impact of this non-overcompensated rear-side emitter, we produced solar cells with and without residual rear side emitter using (i) the same soldering pad paste as above with a 1-5 % wt. amount of Al (paste A) and (ii) an Al-free soldering pad paste (paste B). We varied the area fraction of soldering pads from 0.9 % to 5.5 % and furthermore applied full area screen printing with both soldering pad pastes (area fraction of 100 %). For cells with full-area soldering pad with Al-free paste B, the open-circuit voltage decreases drastically from $V_{oc} = 603$ mV without residual rear-side emitter to $V_{oc} \approx 455$ mV with residual rear-side emitter as can be seen in Fig. 5a. This huge voltage drop can be explained by the rear-side emitter which acts as a second diode connected to the p-n-junction in series and reversed to it. Thus, the drop in open-circuit voltage due to a rear-side emitter may be caused to some

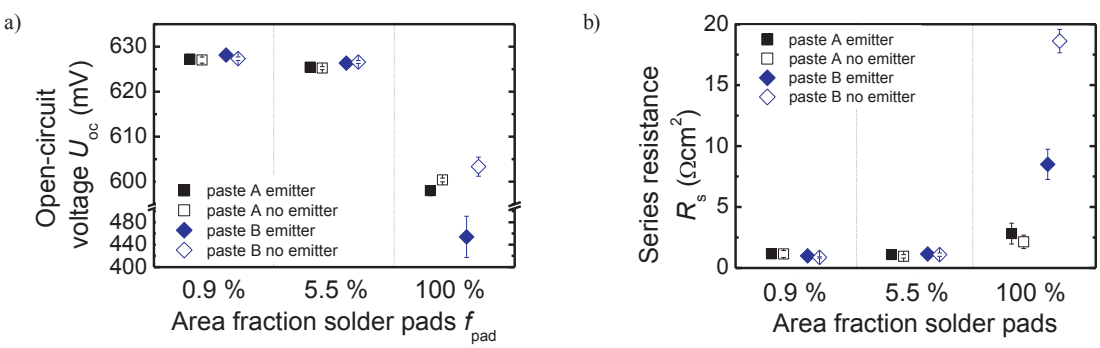

Fig. 5 Performance results of Al-BSF cells with (solid symbols) and without (open crossed) rear side emitter and varying area fraction of the soldering pads, screen printed with paste A (black squares) and paste B (blue diamonds). a) The open-circuit voltage of the cells slightly decreases for all groups when increasing the area fraction of the soldering pads from 0.9 % to 5.5 % and drops drastically for a full area soldering pad, especially for cells with paste B (Al-free) and a rear side emitter. b) For cells with a full area soldering pad the series resistance increases. The strongest increase is found for paste B (Al-free) especially if the cells have no residual emitter on the rear side.

extent by the n-p-junction's reverse open-circuit voltage on the rear side. However, for paste A (with 1-5 % wt. Al share) the open-circuit voltage only drops from V_{oc} = 600 mV without residual rear-side emitter to V_{oc} = 598 mV with residual rear side emitter, which is rather small.

A further reason causing the difference in the behaviour of the Al-free and Al-containing soldering pad paste may be the quality of the contact formed to the base. Fig. 5b shows the series resistance of the cells. While no significant differences between the two pastes can be seen for 0.9 % and 5.5 % area fraction of soldering pads, the series resistance for cells with full area soldering pad increases dramatically for paste B (Al-free), especially for cells without residual rear side emitter. This indicates an improved contact formation for paste A (Al-containing), which we ascribe to the partial Al-alloying from the Al share in the paste. To understand these differences in the contact resistance, the description of the back contact with a Schottky diode and a shunt resistance in parallel to the Schottky diode, as proposed by Green et al. [20] is helpful. For the improved contact quality of paste A compared to paste B, a lower shunt resistance, due to the partial Al-alloying may be the cause. For paste B on the other hand, spiking of silver may be determinant for a high shunt resistance in the back contact model, so that the overall contact resistance of the Schottky diode and the parallel shunt resistance increases resulting in an inferior contact quality compared to paste A. Since the influence of the Schottky diode on the contact resistance increases for paste B, a residual rear side emitter has beneficial effect on the contact quality due to the increased surface doping concentration, which leads to a decrease in the barrier height of the metal semiconductor system.

5. Conclusion

We measured the saturation current density $J_{o,pad}$ at the silicon surface under soldering pads which amounts to $26.7 \cdot 10^3$ and $85.4 \cdot 10^3$ fA/cm^2 depending on the surface conditions, which is 90 to 280 times higher than the saturation current density of Al-doped p^+-regions. For Al-BSF cells with soldering pads up to an area fraction of 6.2 %, the effects on the open-circuit voltage induced by recombination underneath the soldering pads can be described sufficiently by the measured saturation current densities. Within a microstructural SEM analysis it has been found that the Al-alloying from the 1-5 % wt. Al-share in the soldering pad paste only occurs partially, which leads to regions with non-compensated residual rear-side emitter.

In order to investigate how a non-overcompensated emitter under soldering pads behaves, solar cells with full area soldering pads with and without a rear-side emitter are produced. Using an Al-containing and an Al-free soldering pad paste for the full area metallization, it is demonstrated that the partial Al-alloying from the Al-share in the soldering pad paste is able to overcompensate a rear-side emitter which is not the case for the Al-free soldering pad paste. Concerning both, overcompensation of the rear-side emitter and contact quality of cells with full area soldering pads, a different behavior is observed for Al-free and Al-containing soldering pad pastes, which will be further investigated.

Acknowledgements

This work was partially funded by an internal program of the Fraunhofer society and the German Ministry for the Environment, Nature Conservation and Nuclear Safety (BMU) under the frame of the project QUASSIM (0325132A).

The authors would like to thank the PV-TEC team at Fraunhofer ISE, especially A. Spribille and D. Erath for solar cell processing and J. Greulich, M. Rauer and R. Woehl for fruitful discussions.

References

[1] J. Krause, et al., "Microstructural and electrical properties of different-sized aluminum-alloyed contacts and their layer system on silicon surfaces." Solar Energy Materials and Solar Cells 95(8): 2151-60 (2011).

[2] V. Meemongkolkiat, et al., "Factors limiting the formation of uniform and thick aluminium-back-surface field and its potential." Journal of the Electrochemical Society 153(1): 53-58 (2006).

[3] F. Huster, "Investigation of the alloying process of screen printed aluminium pastes for the BSF formation on silicon solar cells", Proceedings of the 20th EPVSEC, Barcelona, Spain. 2005.

[4] D. Kray, et al., "Reducing Ag-cost and increasing efficiency. Multicrystalline silicon solar cells with direct plated contacts exceeding 17 % efficiency", Proceedings of the 26th EPVSEC, Hamburg, Germany 2011.

[5] D. E. Kane and R.M. Swanson, "Measurement of the emitter saturation current by a contactless photocnductivity decay methods (silicon solar cells)", Proceedings of the 18th IEEE Specialists Conference, Las Vegas, Nevada, USA 1985.

[6] R. A. Sinton and A. Cuevas, "Contactless determination of current-voltage characteristics and minority carrier lifetimes in semiconductors from quasi-steady-state photoconductance data", Applied Physics Letters, 1996. 69(17): p.2510-12.

[7] M. Rüdiger et al., "Effect of incomplete ionization for the description of highly aluminium-doped silicon", Journal of Applied Physics , 2011. 110: p. 024508.

[8] M. Rauer, et al., "Simplifying the manufacturing of n-type silicon solar cells with screen-printed aluminium-alloyed rear emitter". Proceedings of the 25th EPVSEC, Valencia, Spain, 2010.

[9] A.B. Sproul, "Dimensionless solution of the equation describing the effect of surface recombination on on carrier decay in semiconductors", Journal of Applied Physics, 1994. 76(5): p. 2851-4

[10] M.J. Kerr and A. Cuevas,, "General parametrization of Auger recombination in crystalline silicon", Journal of Applied Physics, 2002. 91(4): p. 2473-80

[11] J. del Alamo, J. Van Meerbergen, et al. (1981). "High-low junctions for solar cell applications." Solid-State Electronics 24(6): 533-538.

[12] D. Biro, et al, "Thermal oxidation as a key technology for high efficiency screen printed industrial silicon solar cells", Proceedings of the 34th IEEE PVSC, Philadelphia, USA, 2009

[13] A. Schneider, et al., "Comparison of gettering effects during phosphorus diffusion for one- and double-sided emitters" Proceedings of the 31st IEEE PVSC, Florida, USA, 2005

[14] S. Rein, et al., "Investigation of carrier lifetime in p-type Cz-silicon: specific limitations and realistic prediction of cell performance", Proceedings of the 28th IEEE PVSC, Anchorage, Alaska, USA, 2000.

[15] A. Wolf, D. Biro, et al. (2010). "Comprehensive analytical model for locally contacted rear surface passivated solar cells." Journal of Applied Physics 108(124510): 1-13.

[16] T. Fellmeth, A. Born, et al. (2011). "Recombination at metal-emitter interfaces of front contact technologies for highly efficient silicon solar cells", Proceedings of the 1st International Conference on Silicon Photovoltaics, Freiburg, Germany, Elsevier Energy Procedia.

[17] Bock, R., J. Schmidt, et al. (2008). "Electron microscopy analysis of crystalline silicon islands formed on screen-printed aluminum-doped p-type silicon surfaces." Journal of Applied Physics 104(4): 1-5.

[18] R. W.Olesinski, et al., "The Ag-Si (Silver-Silicon) System", Bulletin of Alloy Phase Diagrams Vol. 10 No.6 1989

[19] A. McAlister, Bull. Alloy Phase Diagrams 8, 526 (1987).

[20] M.A. Green A.W. Blakers, J.Zhao, A.M. Milne, A. Wang and X. Dai, "Characterization of 23-percentefficient silicon solar cells", IEEE Transactions on Electron Devices, Vol. 37, pp. 331-336, 1990